ELSEVIER

Catalysis Today 50 (1999) 299–308

CATALYSIS TODAY

Studies of the oxygen release reaction in the platinum–ceria–zirconia system

Carla E. Hori[1,b], Alan Brenner[a], K.Y. Simon Ng[b], Kenneth M. Rahmoeller[c], David Belton[2,c,*]

[a]*Department of Chemistry, Wayne State University, Detroit, MI, USA*
[b]*Department of Chemical Engineering, Wayne State University, Detroit, MI, USA*
[c]*Physics and Physical Chemistry Department, General Motors R & D, Warren, MI, USA*

Abstract

The relative rates of the CO+oxygen storage material (OSM)$\Rightarrow CO_2$ reaction (R_{CO_2}) and the amounts of rate enhancement obtained upon Pt promotion were examined for ceria and ceria–zirconia OSM. The effect of Pt surface area on R_{CO_2} was decoupled from metal–oxide surface area by pre-sintering the oxides prior to Pt deposition. We find that R_{CO_2} is linearly dependent on Pt area over Pt/CeO_2, but over $Pt/Ce_{0.75}Zr_{0.25}O_2$, the rate is independent of Pt surface area above a threshold surface area. Although Pt sinters more readily on the $Ce_{0.75}Zr_{0.25}O_2$ support, the dispersion effect is more than compensated by the enhanced availability of ''bulk'' O^{2-} within the $Ce_{0.75}Zr_{0.25}O_2$ particles. Furthermore, this study demonstrates that, on a unit surface area basis, the ceria–zirconia support is at least two times more active for the oxygen release reaction than the pure ceria support when the materials are slightly reduced. It is also shown that O^{2-} diffusion is not rate-limiting for the ceria reduction reaction when the reaction is carried out in the kinetically limited regime at 500°C with CO as the reductant.

Keywords: Oxygen storage; Ceria; Ceria–zirconia; Doped ceria; Platinum; Environmental

1. Introduction

One of the most important commercial applications of CeO_2 is as an ''oxygen storage'' component in automotive catalysts. Having ceria to ''store'' (as CeO_2) and ''release'' (as CO_2 or H_2O) oxygen is an efficient way to buffer air-to-fuel ratio (A/F) transients that occur in automotive exhaust under normal operating conditions. Thus, a ceria-containing catalyst that receives a rapidly cycled exhaust gas feedstream that averages out as stoichiometric over time can function as efficiently as if it receives a steady state stoichiometric feed. However, the oxygen storage function in ceria based catalysts is prone to deactivate at temperatures above 800°C. Recognition of the importance of ceria deterioration in catalyst performance has given rise to considerable efforts to stabilize the oxygen storage properties of ceria [1–4]. One approach to achieve more thermally stable materials is to modify the ceria by doping it with other oxides, such as La_2O_3 and Ga_2O_3 [5,6]. Most recently ZrO_2 has been recognized as perhaps the most effective

*Corresponding author. E-mail: nzllsk@powertrain.mpg.gm.com

[1]Current address: Universidade Federal de Uberlandia, Brazil.

[2]Current address: General Motors Powertrain, Milford Proving Grounds, Milford, MI, USA.

0920-5861/99/$ – see front matter
PII: S0920-5861(98)00511-2

dopant for ceria [7–17]. The benefits of ZrO_2 incorporation in automotive catalysts are most pronounced when CeO_2 and ZrO_2 form predominantly a solid solution [12].

Our previous work [12] in this area focused on the characterization of $Ce_xZr_{1-x}O_2$ ($x \leq 1$), oxygen storage materials (OSM) by X-ray diffraction (XRD) and pulsed measurements of oxygen storage capacity (OSC). We showed that the OSC of $Pt/Ce_xZr_{1-x}O_2$ catalysts was 2–5 times higher than the Pt/CeO_2 catalysts when both catalysts were aged above 800°C. In those catalysts, both the OSM and the Pt sintered simultaneously; therefore, it was impossible to isolate the effects of Pt promotion from those inherent to the OSM. In this paper, we de-coupled oxide degradation from Pt sintering in the following manner. First, the OSM were calcined at 950°C prior to Pt deposition. This calcination stabilized the BET surface area and OSC against further degradation at or below 950°C. Next, Pt was added to the OSM with high initial Pt surface areas. A series of kinetic measurements of the $CO+2CeO_2 \Rightarrow Ce_2O_3+CO_2$ oxygen release reaction were made. Aging at successively higher temperatures then decreased the Pt surface areas; both CO chemisorption and kinetic measurements were done following each aging step. This procedure de-coupled oxide sintering from Pt sintering, allowing us to assess the amount of Pt that was 'enough' to fully promote the release reaction. We could also evaluate the rate enhancement achieved by Pt promotion, and understand how ceria and ceria–zirconia differ in their interaction with Pt. Although there have been many studies showing that ceria–zirconia has higher OSC than ceria, this is the first comparison of:

1. the relative rates of the $CO+OSM \Rightarrow CO_2$ reaction (R_{CO_2}) on each material, and
2. the amount of rate enhancement obtained upon Pt promotion.

2. Experimental

2.1. Catalyst preparation

The ceria support was obtained by oven firing of cerium acetate. The $Ce_{0.75}Zr_{0.25}O_2$ solid solution was prepared by dissolving cerium(IV) ammonium nitrate and zirconium nitrate in water at the desired Ce/Zr ratio. Then, the Ce and Zr hydroxides were precipitated by adding excess (~100%) ammonium hydroxide. Finally, the precipitate was washed with deionized water and then calcined in air at 500°C for 1 h in a muffle furnace. Both supports were aged by calcination at 950°C for 24 h in a muffle furnace. After the 24 h calcination procedure, the BET surface areas of CeO_2 and $Ce_{0.75}Zr_{0.25}O_2$ were 7.0 and 7.7 m^2/g, respectively. The purpose of using these pre-calcined supports was to ensure that the oxygen storage properties inherent to the supports would not change during subsequent sintering of Pt. Confirmation that the support materials were insensitive to the redox aging that followed Pt deposition was obtained by showing that the reaction rates measured for the supports after the 24 h calcination remained unchanged by an additional 4 h redox aging at 950°C.

After stabilizing the support materials, 5 wt% Pt was dispersed on the two supports. The addition of Pt was done by five successive adsorptions of H_2PtCl_6. Each adsorption was done using 10 g of support and 50 cc of a solution of H_2PtCl_6 in acetone with 0.002 g of Pt/cm^3. The powder and solution were stirred with a magnetic bar for 4 h. Next, the powder was filtered and dried at room temperature. After each adsorption, the samples were calcined at 500°C in a muffle furnace for 2 h and then placed in a tube furnace at 400°C in flowing H_2 (5% in N_2) for 6 h. We note that after each of the five successive anion adsorptions the Pt dispersion remained constant at roughly 40%. Thus, this method was remarkably effective in depositing more particles of the same size without growing the existing particles larger.

After Pt deposition, the freshly impregnated catalyst material (10 g) was then divided into 1 g lots and aged at the temperatures shown in Table 1. Aging was done in a tube furnace at successively higher temperatures to decrease the Pt dispersion. With the catalyst in the furnace at an elevated temperature, the inlet of the furnace was cycled (0.1 Hz) between 5% O_2/N_2 and 5% H_2/N_2. The gas stream was saturated with water at room temperature before entering the furnace. Pt dispersions in Table 1 were measured using CO chemisorption. Table 1 data show that the initial Pt dispersions were very similar on both supports.

Table 1
Pt dispersions, average crystallite sizes and surface areas determined by CO chemisorption

CO chemisorption results			
Samples	Dispersion (%)	Average crystallite size (Å)	Pt surface area (m^2/g)
Pt/CeO_2			
Fresh	43.1	32	0.450
Aged at 800°C	21.8	62	0.228
Aged at 900°C	18.2	75	0.191
Aged at 950°C	10.5	130	0.110
$Pt/Ce_{0.75}Zr_{0.25}O_2$			
Aged at 700°C	43.5	31	0.473
Aged at 775°C	33.8	40	0.368
Aged at 800°C	15.5	88	0.169
Aged at 900°C	11.7	116	0.128
Aged at 950°C	2.4	579	0.025

2.2. Characterization measurements

The BET surface area measurements were carried out using a multi-function reactor system (RXM-100 from Advanced Scientific Design). For the BET measurements we used approximately 0.5 g of catalyst. The sample was evacuated overnight at room temperature, then cooled to 77 K using liquid N_2 at which point N_2 adsorption was measured. The same reactor system was also used for the Pt surface area determinations using CO chemisorption. In this case the samples were pretreated in a flow of pure H_2 (20 cm^3/min) at 300°C for 1 h and then evacuated at this temperature for at least 2 h. The adsorption of CO was measured by a pulse technique at 300 K. Pure supports adsorbed only negligible amounts of CO which is attributed to the fact that they had very low surface area. Pt particle sizes were estimated by assuming hemispherical particles.

The CO_2 formation rate data were obtained in a flow-through reactor. The inlet of the reactor was connected to a series of four microvalves that allowed different gas streams to be fed to the sample. A gas stream containing 0.5% O_2 in N_2 was used to oxidize the samples. Mixtures of CO and CO_2 in N_2 were also available at concentration ranges varying from 0.125% to 3.5%, as well as a stream of pure N_2 for purging. In these experiments, the typical concentrations were 0.25% for CO_2 (for calibration) and 1% for CO. Fig. 1 graphically describes a typical experiment. A 60 s soak in O_2 at the beginning of each experiment

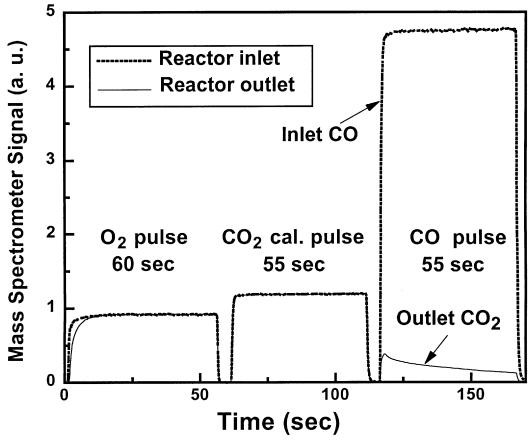

Fig. 1. Sequence of events during the experimental measurement of CO_2 formation rates.

completely oxidizes the OSM. We assume that the stoichiometry of the material after this treatment is CeO_2 and $Ce_{0.75}Zr_{0.25}O_2$. After the O_2 soak, a 50 s pulse of CO_2 was sent through the reactor to calibrate the mass spectrometer. Finally, a 50 s pulse of CO was sent through the reactor. The concentration of generated CO_2 in the gas stream was detected using a quadrupole mass spectrometer. For these measurements 0.04 g of ceria and a flow of 1000 cm^3/min (STP) were used. The same sample was used for measurements at different temperatures. Each measurement was repeated at least three times and the results were averaged. We saw no tendency for the

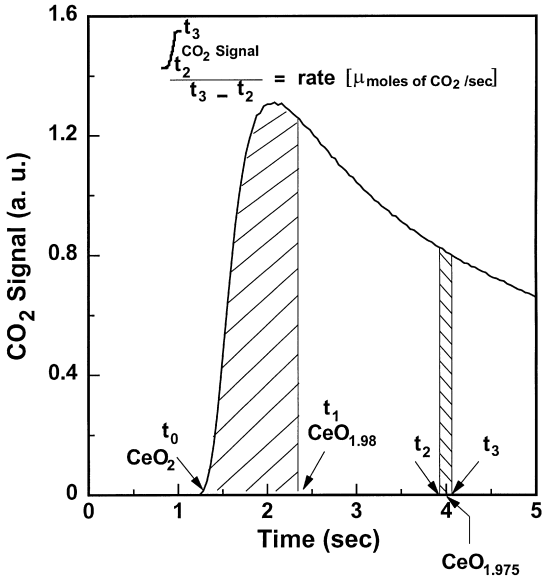

Fig. 2. Schematic representation of the calculation of reaction rates from the raw data.

rates to deteriorate with successive runs suggesting that deactivation, due to carbon build-up, was not confounding our results. Presumably, the oxidation treatment at the end of each reduction removed residual surface carbon (or carbonates). This presumption is supported by the fact that a small amount of CO_2 is generated early in the 60 s oxidation pulse (CO_2 data for the oxidation pulse is not shown in Fig. 1).

Fig. 2 illustrates how the raw data were analyzed to give the rate data reported in this paper. The stoichiometry of the OSM at any time, t_1, was determined by integrating the CO_2 formed from the start of the pulse, t_0, to the time of interest, t_1. Then, the integrated CO_2 formed was mass balanced with the O atoms that left the sample to determine the catalyst stoichiometry at any time. The instantaneous rates for CO_2 formation at a given stoichiometry (between t_2 and t_3) are defined in Fig. 2. Rate data very near the leading edge of the CO pulse was not used in Arrhenius plots, but the integrated CO_2 formed was used for the mass balance. The oxygen release rates measured on the support materials will be symbolized by R_{CO_2} and the rates for Pt promoted samples by $R^{Pt}_{CO_2}$.

In this paper, we only report rates for those conditions where we were clearly not diffusion limited (gas phase and/or pore) or limited by high (>20%) CO conversion. For all catalysts in this study, increasing temperature eventually led to a "roll-over" in R_{CO_2}, where the apparent activation energy (E_a) began to approach zero. We took this roll-over as an indication that a combination of mass transport, pore diffusion and/or high conversion was limiting R_{CO_2}. We avoided those conditions in this study and in doing so defined the upper T limit for reaction over a particular catalyst. The lower T limit was determined by the sensitivity of our mass spectrometer. With these two constraints, not all catalysts could be studied over the same temperature range. Therefore, comparison of the rate over different catalysts was made by extrapolations of the Arrhenius plot to the nearest common temperature. We recognize the potential for errors with such an extrapolation, but feel that it is the best way to compare catalysts in our study.

3. Results and discussion

3.1. Reaction rates over unpromoted OSM

We begin this paper with a discussion of the behavior of the OSM in the absence of Pt promotion. Fig. 3

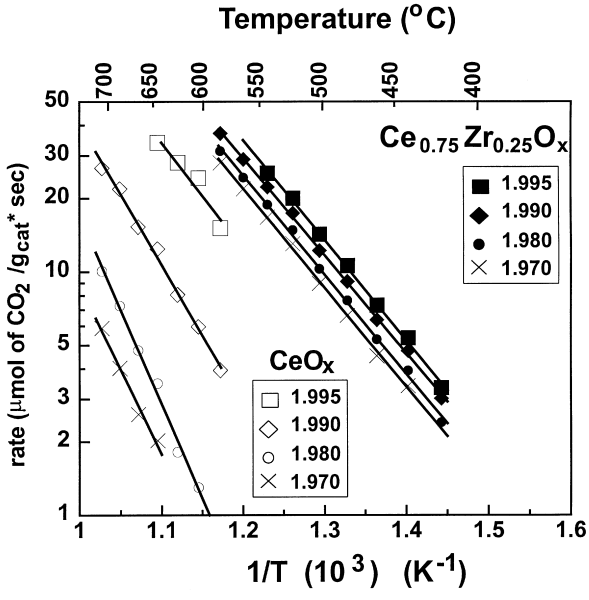

Fig. 3. Arrhenius plots for unpromoted ceria and ceria–zirconia materials at different oxide stoichiometries.

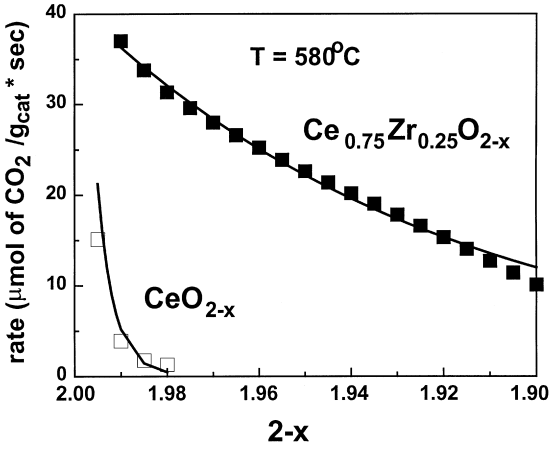

Fig. 4. Reaction rates as a function of oxide stoichiometry for unpromoted ceria and ceria–zirconia materials at 580°C.

shows R_{CO_2} vs. $1/T$ for the support materials at four different levels of reduction between CeO_2 and $CeO_{1.97}$, meaning that less than 6% of the Ce^{+4} was reduced to Ce^{+3}. Fig. 4 summarizes data at 580°C to illustrate the dependence of reaction rate on oxide stoichiometry. In this paper we focus primarily on mildly reduced CeO_x ($2>x>1.970$) materials in order to match the levels of reduction necessary for good conversion efficiencies over fully formulated catalysts [16]. Previous measurements [16] have shown that for an aged catalyst operating in simulated exhaust with A/F perturbations, CO and NO_x begin to break through when the perturbations require more than ~5% of the OSM to store and release oxygen. The aged materials in this study have fairly low (~7.5 m^2/g) surface area; therefore, only about 1.5% of the 'reducible' O is on the surface of the particles (see Appendix A). Thus, after surface reduction of CeO_2, the overall stoichiometry would be $CeO_{1.9925}$ which means that "bulk" oxygen is participating when the oxides are reduced below ~$CeO_{1.992}$.

As shown in Figs. 3 and 4, when the oxygen storage materials are less than 1% reduced, R_{CO_2} is about 2-fold higher over $Ce_{0.75}Zr_{0.25}O_{1.995}$ than over $CeO_{1.995}$. It is important to note that, this level of reduction involves primarily surface oxygen (according to our estimate in Appendix A), the two materials have about the same surface area, and the reaction is taking place in the kinetically limited regime. Thus, under these conditions, we find that $Ce_{0.75}Zr_{0.25}O_{1.995}$ surface is about 2.5 times more active per unit area than $CeO_{1.995}$.

Figs. 3 and 4 also include reaction rates when more than 1% of the ceria was reduced, and based on our estimates of surface O concentrations, both surface and bulk O are involved in the reduction process. For both materials, the reaction slows down as the material is reduced, but the effect is much more pronounced for CeO_{2-x} than for $Ce_{0.75}Zr_{0.25}O_{2-x}$. Fig. 3 data (symbols) were fit (lines) with the parameters shown in Table 2, and Fig. 4 data were fit using the functional forms and parameters shown in Table 3 (see Appendix B). Figs. 3 and 4 data suggest that reaction over $Ce_{0.75}Zr_{0.25}O_2$ and CeO_2 are mechanistically very different. The mechanistic differences are reflected in the Arrhenius behavior shown in Fig. 3. $Ce_{0.75}Zr_{0.25}O_{2-x}$ shows a smooth decay of R_{CO_2} with the level of reduction (Fig. 3) without a significant change in the E_a of the reaction (Table 2), suggesting that similar processes are limiting the reaction rate over the range of stoichiometry in Fig. 3. In contrast, CeO_{2-x} shows that E_a increases dramatically as the material is reduced, suggesting that different processes control the rate as the material is slightly reduced. In CeO_2, those species that react rapidly early in the reduction process are severely depleted when CeO_2 is reduced to $CeO_{1.98}$.

The observed differences in x-dependence of the two OSM suggests that while $Ce_{0.75}Zr_{0.25}O_{2-x}$ behaves as a reasonably homogeneous material, CeO_{2-x} can be better described as having a small amount of very reducible material along with the large fraction which is much less reducible. This conclusion fits well with the previous TPR work which showed a continuum of ceria–zirconia reduction over the temperature range of this study [7]; but only a small fraction of ceria being reducible [7,8]. At these temperatures, the behavior of CeO_{2-x} is well described by either having only the surface being reducible or having a minority of more reducible (typically thought of as small) particles.

Figs. 3 and 4 data show no sharp distinction between surface and bulk oxygen in the $Ce_{0.75}Zr_{0.25}O_2$ materials. In our previous paper, [12] we argued against the idea [8,18] that Zr incorporation was beneficial because it enhanced bulk O^{2-} diffusion

Table 2
Regression parameters from the reaction rate data for samples supported on ceria and on ceria–zirconia

Regression analysis for rate data in Figs. 3, 6, 7 Rate=$A\exp(-E_a/RT)$			
X	A	E_a[a]	Pt area
CeO_2 samples with and without added Pt			
CeO_x (Fig. 3)			
1.995	2.2×10^6	20.2	
1.990	2.5×10^7	26.7	
1.980	1.0×10^9	35.8	
1.970	9.1×10^7	32.3	
$Pt/CeO_{1.990}$ (Fig. 6)			
	1.7×10^7	26.0	0
	6.5×10^8	23.6	0.450
	8.9×10^4	13.3	0.228
	2.5×10^5	15.8	0.191
	7.0×10^6	21.7	0.128
$Pt/CeO_{1.975}$ (Fig. 7)			
	1.6×10^8	33.0	0
	1.0×10^{14}	54.6	0.450
	5.9×10^9	37.6	0.228
	8.2×10^{11}	47.4	0.191
	2.2×10^{12}	49.8	0.128
$Ce_{0.75}Zr_{0.25}O_2$ samples with and without added Pt			
$Ce_{0.75}Zr_{0.25}O_x$ (Fig. 3)			
1.995	3.0×10^6	18.9	
1.990	1.8×10^6	18.4	
1.980	1.9×10^6	18.8	
1.970	1.7×10^6	18.7	
$Pt/Ce_{0.75}Zr_{0.25}O_{1.990}$ (Fig. 6)			
	1.8×10^6	18.4	0
	1.5×10^7	14.1	0.473
	6.0×10^7	16.2	0.368
	5.7×10^7	16.3	0.169
	4.9×10^{10}	24.7	0.128
	1.1×10^{11}	27.5	0.025
$Pt/Ce_{0.75}Zr_{0.25}O_{1.975}$ (Fig. 7)			
	1.5×10^6	18.5	0
	1.2×10^{12}	26.9	0.473
	8.2×10^9	22.0	0.368
	1.0×10^{10}	22.6	0.169
	1.7×10^{11}	26.7	0.128
	3.7×10^{11}	29.6	0.025

[a]kcal/mol.

rates. Instead we favor associating the improved reducibility of the Zr promoted materials with an increase in the solubility of anion vacancies in the α-phase (solid solution of vacancies) of non-stoichiometric ceria (see Ref. [21] for a phase diagram). Despite some differences in the mechanistic details, we are in agreement [8,18–20] with the important concept that Zr modifies the bulk properties of ceria to make the interior of the ceria particles more reducible.

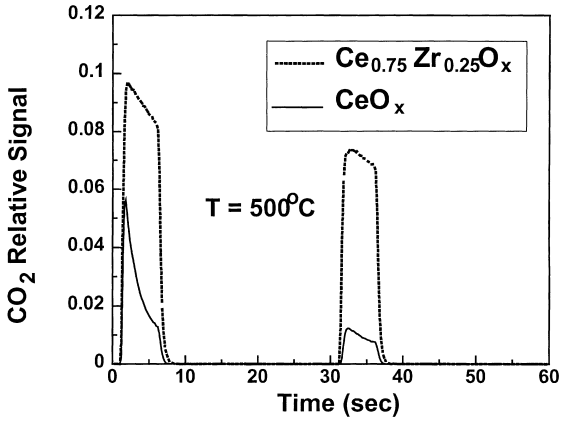

Fig. 5. Measurement of CO_2 evolution during an experiment designed to determine the importance of O^{2-} diffusion in the reaction rates. Note that the reaction rates continue at the same point that they stopped after a 25 s delay.

In order to test whether or not the CO+OSM⇒CO_2 reaction rate is O^{2-} diffusion limited, we modified the experiment described in Fig. 1, to that shown in Fig. 5. In the modified experiment, after oxidation of the OSM and calibration of the mass spectrometer, we injected a short pulse of CO (5 s) followed by a long purge of N_2 (25 s), and then another pulse of CO. If diffusion of O^{2-} to the surface is rate-limiting then during the CO pulse the surface will be depleted of reducible oxygen atoms thus establishing a diffusion gradient. When CO is removed from the gas phase, oxygen from the bulk should diffuse against the gradient, and in so doing increases the surface oxygen content. Thus, the CO_2 formation rate would increase when the CO is re-introduced to the gas stream. Fig. 5 shows that after the 25 s purge in N_2 the CO_2 formation rate does not increase, but instead the reaction resumes at the point where it left off when the gas phase CO was removed. Thus, more ''surface'' oxygen has not been generated through diffusion, meaning that diffusion of O^{2-} is not what limits the reaction rate measured in the kinetically limited regime when CO is used as the reductant. These experiments sup-

Table 3
Parameters from the 3D curve fits of the reaction rate data for samples supported on ceria and on ceria–zirconia

Parameters from curve fits of reaction rates					
Samples	a	b	c	d	r^2
Samples supported on CeO_2					
Rate=$\exp(a+b(2-x)/T+c(2-x)^2/T^2+d(2-x))$[a]					
CeO_2 (0 m^2 Pt/g)	4.585	-1.165×10^6	1.842×10^9	1046.943	0.99086
Pt/CeO_2 (0.45 m^2 Pt/g)	2.071	2.865×10^5	-2.133×10^{10}	167.639	0.99748
Pt/CeO_2 (0.23 m^2 Pt/g)	5.304	-6.735×10^5	-9.757×10^8	628.224	0.99165
Pt/CeO_2 (0.19 m^2 Pt/g)	5.632	-7.764×10^5	1.795×10^9	630.014	0.99136
Pt/CeO_2 (0.13 m^2 Pt/g)	5.498	-8.501×10^5	1.800×10^9	723.784	0.99076
Samples supported on $Ce_{0.75}Zr_{0.25}O_2$					
Rate=$\exp(a+b(2-x)/T+c(2-x)/T^2+d/T^2)$[a]					
$Ce_{0.75}Zr_{0.25}O_2$ (0 m^2 Pt/g)	8.370	2.341×10^3	-1.097×10^7	-3.388×10^6	0.99593
$Pt/Ce_{0.75}Zr_{0.25}O_2$ (0.47 m^2 Pt/g)	8.683	7.574×10^4	-5.353×10^7	-1.369×10^6	0.98722
$Pt/Ce_{0.75}Zr_{0.25}O_2$ (0.37 m^2 Pt/g)	8.903	6.157×10^4	-4.360×10^7	-1.602×10^6	0.99066
$Pt/Ce_{0.75}Zr_{0.25}O_2$ (0.17 m^2 Pt/g)	9.177	5.135×10^4	-4.010×10^7	-1.710×10^6	0.99424
$Pt/Ce_{0.75}Zr_{0.25}O_2$ (0.13 m^2 Pt/g)	11.836	5.000×10^4	-3.944×10^7	-2.764×10^6	0.99274
$Pt/Ce_{0.75}Zr_{0.25}O_2$ (0.025 m^2 Pt/g)	13.396	1.766×10^4	-2.313×10^7	-3.786×10^6	0.99633

[a] x is the degree of reduction of the material and T is the temperature in Kelvin.

port our previous idea that a process other than O^{2-} diffusion that limiting the reduction rate in one of these materials [12]. However, we recognize that these conclusions apply only to the conditions of our experiment. Thus, the reaction could be O^{2-} diffusion limited when carried out at temperatures above or below 500°C, or when hydrogen is the reductant, or when the materials are more highly reduced.

3.2. *Effect of Pt promotion of the OSM on CO_2 formation rates*

It is widely recognized that the addition of precious metals (PM) to OSM enhances their performance. In this section, we quantify the effect of Pt promotion, by adding Pt to the pre-sintered OSM at reasonably high (~43%) initial Pt dispersions. After Pt deposition, the catalysts were aged at successively higher temperatures, and the Pt dispersions were determined. Table 1 data show that, after a low temperature (800°C) aging, Pt dispersions were higher on CeO_2 than on $Ce_{0.75}Zr_{0.25}O_2$. As the materials were aged, the trend to higher Pt dispersions on CeO_2 continued, so that after aging at 950°C, the dispersion of Pt on CeO_2 was about 4-fold greater than that of Pt on $Ce_{0.75}Zr_{0.25}O_2$. Thus, we conclude that maintenance of higher PM dispersions is not one of the reasons that ceria–zirconia solid solutions make superior OSM. For the remainder of this paper, the most important point to take from the dispersion measurements is that Pt surface area was varied without significant change in the support material (see Section 2 for confirmation).

After establishing the Pt surface area in the CeO_2 and $Ce_{0.75}Zr_{0.25}O_2$ catalysts, $R^{Pt}_{CO_2}$ was measured in the kinetically limited temperature range. Figs. 6 and 7 show rate data (symbols) at two points in the reduction process. In these figures, the lines are fits of the data using the parameters and functional forms in Table 3. Fitting $R^{Pt}_{CO_2}$ over these materials gives us some insight into the reduction process. Over both materials plots of $R^{Pt}_{CO_2}$ vs. $1/T$ give straight lines at a given oxide stoichiometry, but these data cannot be fit satisfactorily with an $R^{Pt}_{CO_2} = C(x)\exp(-(E_a - B(x))/RT)$ functional form, where $B(x)$ and $C(x)$ are functions describing an ''O'' concentration dependence. Simply put, there is a very strong coupling between the temperature and concentration terms that is not easily described in familiar kinetic terms. In our data, as the temperature is increased, the reaction rate at low ''O'' concentration increases faster than does the reaction rate at high ''O'' concentration. The net effect is that ''more'' oxygen is accessible for reaction as the reaction temperature is

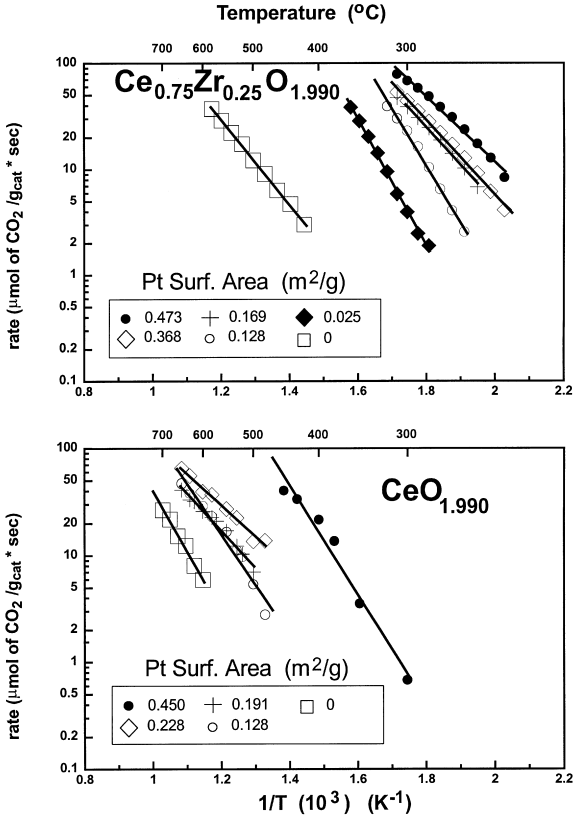

Fig. 6. Arrhenius plots for samples with different Pt surface areas supported on ceria and on ceria–zirconia for an initial state of 2% reduction.

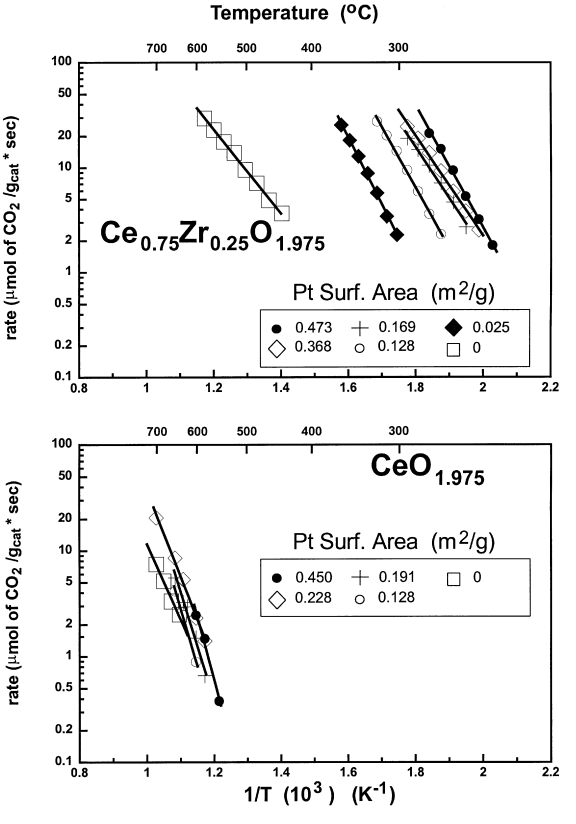

Fig. 7. Arrhenius plots for samples with different Pt surface areas supported on ceria and on ceria–zirconia for an initial state of 5% reduction.

increased, in good agreement with the general shape of the TPR of these materials [7,8,10,18].

In order to quantify the effect of Pt promotion (Fig. 8), we normalized $R^{Pt}_{CO_2}$, the rate over the Pt promoted catalysts, to that over the unpromoted catalysts, R_{CO_2}. In Fig. 8, these ratios $R^{Pt}_{CO_2}/R_{CO_2}$ are reported for CeO_{2-x} at 580°C and for $Ce_{0.75}Zr_{0.25}O_{2-x}$ at 300°C. It was necessary to use different temperatures since the activities for the $Ce_{0.75}Zr_{0.25}O_{2-x}$ samples were much higher than that for the CeO_{2-x} samples. For comparison, the rates for the unpromoted materials were extrapolated to 300°C for $Ce_{0.75}Zr_{0.25}O_2$ and to 580°C for CeO_{2-x}, since their activity at these temperatures was too low to be measured in our experiment. Rates in Fig. 8 are plotted vs. Pt surface area, but the shape of the curves does not change if instead the *x*-axis were Pt perimeter (m Pt).

The addition of Pt to either OSM increases the reaction rate by $\sim 200x$ in the highly oxidized ($2-x=1.990$) materials (Figs. 6 and 8). Therefore, Pt addition did not change the fact that $Ce_{0.75}Zr_{0.25}O_{1.990}$ is ~100-fold more active than $CeO_{1.990}$. Further, decreasing Pt surface area on either OSM primarily increases E_a while decreasing R_{CO_2} (Table 2); however, the dependence of E_a on Pt surface area is very complex for both materials (Fig. 8 and Table 2). Over $Pt/Ce_{0.75}Zr_{0.25}O_{1.990}$ (Fig. 8), $R^{Pt}_{CO_2}$ is not particularly sensitive to Pt surface area unless it falls below about 0.15 m^2/g. Based on Fig. 8 data we conclude that only about 3% of the $Ce_{0.75}Zr_{0.25}O_{1.990}$ surface need be covered with Pt to achieve "full" promotion of this material. $Pt/CeO_{1.990}$ on the other hand, is extremely sensitive to Pt surface area with $R^{Pt}_{CO_2}$ falling 60-fold for a 2-fold decrease in Pt area. It is likely that the breakpoint in $R^{Pt}_{CO_2}$ vs. Pt surface area

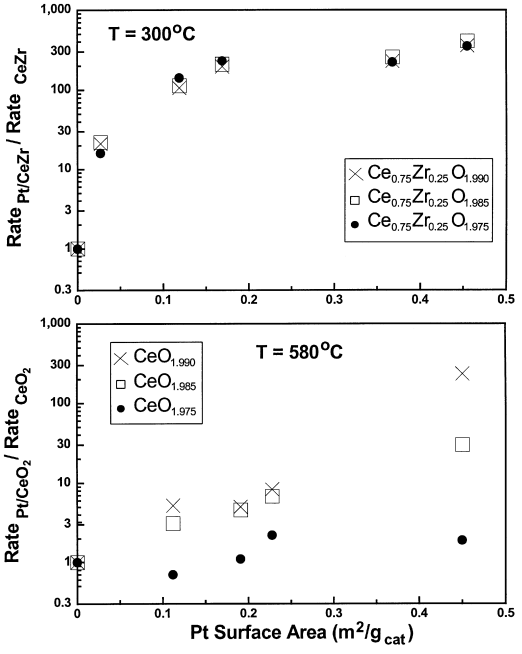

Fig. 8. Degree of Pt promotion obtained for samples supported on ceria and on ceria–zirconia at different degrees of reduction obtained by normalizing $R^{Pt}_{CO_2}$ to R_{CO_2}, at 580°C and 300°C, respectively.

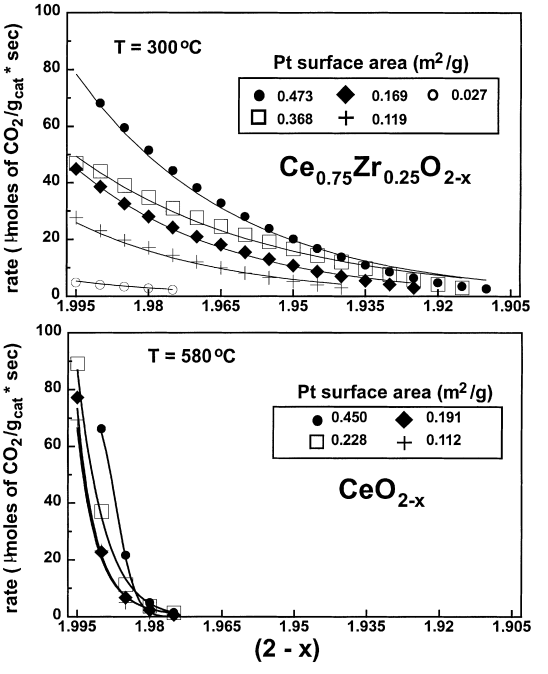

Fig. 9. Functional dependence of the reaction rates on oxide stoichiometry for various Pt surface areas for ceria–zirconia at 300°C and for ceria at 580°C.

occurs at much higher surface Pt areas than we achieved on ceria. Taken together, Fig. 6 and Table 1 data make an interesting point. Pt tends to sinter more readily on $Ce_{0.75}Zr_{0.25}O_x$ than on CeO_x, but because $Ce_{0.75}Zr_{0.25}O_x$ is less sensitive to Pt surface area the enhanced Pt sintering is not as detrimental to the catalyst.

Fig. 7 contains data similar to that in Fig. 6, but at a more advanced stage in the reduction process. For $Ce_{0.75}Zr_{0.25}O_{1.975}$ (Fig. 7), Pt promotes CO_2 formation in a manner quite similar to that in the more heavily oxidized $Ce_{0.75}Zr_{0.25}O_{1.995}$ (Fig. 6). For CeO_x, on the other hand, there is no Pt promotion effect by the time CeO_2 is reduced to $CeO_{1.975}$. Pt/CeO_x is quite similar to CeO_x, in that the reduction reaction appears to occur over a minority species. Thus, this species is relatively quickly extinguished and the reaction essentially stops. This point is best made in lower half of Fig. 9, where $R^{Pt}_{CO_2}$ is plotted vs. x for the Pt/CeO_x. At 580°C, the reaction is essentially over once about 2% of the CeO_2 is reduced. On the other hand, $Pt/Ce_{0.75}Zr_{0.25}O_x$, shows a smooth continuum of reduction. Even when tested at a 280°C lower temperature than Pt/CeO_x, $Pt/Ce_{0.75}Zr_{0.25}O_x$ can be reduced at least seven times more completely.

4. Summary

The kinetic data presented here are to our knowledge the first detailed examination of the rates of "O" release from either promoted or unpromoted ceria and ceria–zirconia in the 10 Torr pressure regime. These data show that when highly oxidized ceria–zirconia is 2.5 times more active on a surface area basis than is ceria. The reaction rates over either OSM decrease as the materials are reduced; however, ceria is much more sensitive to degree of reduction than is ceria–zirconia.

For Pt promoted samples, we observed that Pt supported on ceria maintain higher dispersions than does Pt on ceria–zirconia; therefore, the maintenance of higher Pt dispersions is not a contributor to making ceria–zirconia a better OSM than ceria. Although Pt

dispersion on ceria–zirconia was lower than that on ceria, the Pt/ceria–zirconia catalysts were not as sensitive to Pt surface area as was the ceria based catalysts. Overall, the properties of the OSM and not the interactions with Pt are the dominant factors that make ceria–zirconia a "better" OSM. Finally, we have presented experimental data to support our previous conclusion [12] that diffusion of O^{2-} from the bulk to surface is not the rate-limiting process in the reduction of these materials when CO is used as the reductant at 500°C. These measurements further support our idea that it is the solubility of anion vacancies in the oxide lattice that limits the "bulk" reducibility of these materials' under the conditions that we have employed.

Appendix A

Calculation of surface oxygen concentration

Considering the ceria reduction reaction, we have

$$2CeO_2 + CO \Rightarrow CO_2 + Ce_2O_3$$

$$\frac{1\,\text{mol}}{172\,\text{g}} \times \frac{\text{mol of 'O'}}{2\,\text{mol of } CeO_2} \times \frac{10^6\,\mu\text{mol}}{1\,\text{mol}} = \frac{2907\,\mu\text{mol}}{\text{g}}.$$

We calculated the number of 'O' atoms that can be pulled from the surface by using the lattice parameter of cubic ceria (5.34 Å) and the average surface area of our materials (7.3 m^2/g). We assumed that 1/4 of the 'O' at the surface can be pulled out

$$\frac{1\text{'O'}}{(5.34)^2\ \text{Å}^2} \times \frac{10^{20}\ \text{Å}^2}{1\,\text{m}^2} \times \frac{1\,\text{mol}}{6.023 \times 10^{23}\,\text{atoms}}$$

$$\times \frac{10^6\,\mu\text{mol}}{1\,\text{mol}} \times \frac{7.3\,\text{m}^2}{\text{g}} = 42.6\,\mu\text{mol of surface 'O'/g}.$$

The ratio of surface 'O'/total 'O' give us

$$\frac{42.6\,\mu\text{mol of surface 'O'/g}}{2907\,\mu\text{mol/g}} \times 100 = 1.44\%.$$

Appendix B

Curve fitting of experimental data

Given that very little rate data exists for these materials, we decided to report a rate expression that can describe all the data in this paper. We make no attempt to ascribe these parameters to any type of elementary step and/or process, but these functions do provide a way to calculate the reaction rate. We suspect that in the future these rate expressions may prove useful for math modeling of reactions over ceria-based catalysts. For a given catalyst, data at all degrees of reduction (x) and temperature were fit simultaneously using a 3D fitting routine. We note that a different functional form (see Table 3) was required to describe the behavior for both materials.

References

[1] K.C. Taylor, Catal. Rev.-Sci. Eng. 35 (1993) 433.
[2] A. Trovarelli, Catal. Rev.-Sci. Eng. 38 (1996) 439.
[3] M. Shelef, G.W. Graham, Catal. Rev.-Sci. Eng. 36 (1994) 433.
[4] J.T. Kummer, J. Phys. Chem. 90 (1986) 4747.
[5] B.K. Cho, J. Catal. 131 (1991) 74.
[6] T. Mikki, T. Ogawa, M. Haneda, N. Kakuta, A. Ueno, S. Tateishi, S. Matsuura, M. Sato, J. Phys. Chem. 94 (1990) 6464.
[7] T. Murota, T. Hasegawa, S. Aozasa, H. Matsui, M. Motoyama, J. Alloys Comp. 193 (1993) 298.
[8] P. Fornasiero, R. Di Monti, G. Ranga Rao, J. Kaspar, S. Meriani, A. Trovarelli, M. Graziani, J. Catal. 151 (1995) 168.
[9] M. Ozawa, M. Kimura, A. Isogai, J. Alloys Comp. 193 (1993) 73.
[10] C. de Leitenburg, A. Trovarelli, J. Llorca, F. Cavani, G. Bini, Appl. Catal. A 139 (1996) 161.
[11] J.G. Nunan, W.B. Willianson, H.J. Robota, SAE paper #960798.
[12] C.E. Hori, H. Permana, K.Y.S. Ng, A. Brenner, K. More, K.M. Rahmoeller, D.N. Belton, Appl. Catal. B 16 (1998) 105.
[13] L. Muβmann, D. Lindner, E.S. Lox, R. van Yperen, T.P. Kreuser, I. Mitsushima, S. Taniguchi, G. Garr, SAE paper #970465.
[14] J.G. Nunan, SAE paper #970467.
[15] J.P. Cuif, G. Blanchard, O. Touret, A. Seigneurin, M. Marczi, E. Quéméré, SAE paper #970463.
[16] H. Permana, D.N. Belton, K.M. Rahmoeller, S.J. Schmieg, C.E. Hori, K.Y.S. Ng, A. Brenner, SAE paper #970462.
[17] T. Egami, W. Dmowski, R. Brezny, SAE paper #970461.
[18] F. Zamar, A. Trovarelli, C. de Leitenburg, G. Dolceti, Stud. Surf. Sci. Catal. 101 (1996) 1283.
[19] G. Balducci, J. Kaspar, P. Fornasiero, M. Graziani, M.S. Islam, J.D. Gale, J. Phys. Chem. B 101 (1997) 1750.
[20] P. Fornasiero, G. Balducci, R. Di Monte, J. Kaspar, V. Sergo, G. Gubitosa, A. Ferrero, M. Graziani, J. Catal. 164 (1996) 173.
[21] M. Ricken, J. Nolting, I. Riess, J. Solid State Chem. 54 (1984) 89.